Interaction of Ascorbate Peroxidase with Substrates: A Mechanistic and Structural Analysis†

Isabel K. Macdonald,‡ Sandip K. Badyal,‡ Lila Ghamsari,‡,§ Peter C. E. Moody,‖ and Emma Lloyd Raven*,‡

Department of Chemistry, University of Leicester, University Road, Leicester LE1 7RH, U.K., and Department of Biochemistry and Henry Wellcome Laboratories for Structural Biology, Henry Wellcome Building, University of Leicester, Lancaster Road, Leicester LE1 9HN, U.K.

Received April 7, 2006

ABSTRACT: Previous work [Sharp, K. H., et al. (2003) *Nat. Struct. Biol. 10*, 303−307] has revealed the location of the ascorbate binding site in ascorbate peroxidase and has identified hydrogen-bonding interactions to Arg172, Lys30, and the heme 6-propionate as important in formation of the enzyme−substrate complex. In this work, the individual and collective contributions of these hydrogen bond interactions have been dissected using site-directed mutagenesis, steady-state and pre-steady-state kinetics, X-ray crystallography, and modified substrate analogues. Steady-state and pre-steady-state kinetic data reveal that the hydrogen bonds to Arg172 and the heme 6-propionate play a major part in stabilization of the bound ascorbate but that the interaction with Lys30 plays only a minor role. Binding of aromatic substrates is not affected by substitutions at Arg172/Lys30. Neutralization or removal of electrostatic charge at (Lys30) or adjacent to (Lys31) the ascorbate site does not substantially disrupt the binding interaction. Substrate oxidation and reduction of Compounds I and II is still possible in the absence of Arg172, but at a much reduced level. Crystallographic data (to 1.8 Å) for the R172A variant indicate that the molecular structure of the proposed [Sharp, K. H., et al. (2004) *Biochemistry 43*, 8644−8651] proton transfer pathway from the ascorbate to the heme is conserved, which accounts for the residual activity. The results are discussed in terms of our wider understanding of the structural features that control substrate binding specificity in other peroxidase enzymes.

Ascorbate peroxidases are class I (*1*) heme peroxidases that catalyze the H_2O_2-dependent oxidation of L-ascorbate in plants, algae, and certain cyanobacteria. The catalytic mechanism involves formation of an oxidized Compound I intermediate that is subsequently reduced by the substrate (ascorbate) in two, successive single electron transfer steps (eqs 1−3, where HS = substrate and $S^\bullet$ = one electron oxidized form of the substrate). APX[1] enzymes show high

$$\text{APX} + \text{H}_2\text{O}_2 \xrightarrow{k_1} \text{Compound I} + \text{H}_2\text{O} \quad (1)$$

$$\text{Compound I} + \text{HS} \xrightarrow{k_2} \text{Compound II} + \text{S}^\bullet \quad (2)$$

$$\text{Compound II} + \text{HS} \xrightarrow{k_3} \text{APX} + \text{S}^\bullet + \text{H}_2\text{O} \quad (3)$$

specificity for L-ascorbate as electron donor but will also oxidize nonphysiological (usually organic) substrates that are characteristic of the class III peroxidases, in some cases at rates comparable to that of ascorbate itself (*2*−*4*). It is not yet known whether the oxidation of aromatic substrates by APX has a physiological role. Recent work (*5*, *6*) has shed new light on these substrate binding interactions. Hence, it is now established that there are two substrate binding sites in APX, one for ascorbate and a second site for binding of aromatic substrates. The structure of the APX−ascorbate complex (*6*) shows that the anionic substrate is bound to the enzyme through electrostatic interactions to positively charged residues close to the so-called γ-heme edge (Figure 1). There are three hydrogen bonds: between the 2-OH and 3-OH groups of the substrate (Scheme 1) and Arg172; between the 2-OH group and the (deprotonated) heme 6-propionate; and between the 6-OH group and Lys30. This structure helped to rationalize the unexpected observation (*7*) that APX does not utilize Trp179 in its Compound I intermediate, because there is direct coupling of the substrate to the heme through the heme 6-propionate, completely bypassing Trp179; this is in direct contrast to cytochrome *c* peroxidase (C*c*P), which uses the equivalent residue (Trp191) during catalysis as part of an electron transfer pathway from the substrate to the heme of Compound I (*8*). The second binding site is used by aromatic substrates (e.g., guaiacol, *p*-cresol), but its location has not been unambiguously confirmed. The best available information comes from crystallographic work (*5*)

† This work was supported by grants from BBSRC (Grant 91/B19083 and studentship to S.K.B.), The Leverhulme Trust (Grant RF/RFG/2005/0299 to E.L.R.), and The British Council (traveling fellowship to L.G.).

* To whom correspondence should be addressed. Telephone: +44 (0)116 229 7047. Fax: +44 (0)116 252 2789. E-mail: emma.raven@le.ac.uk.

‡ Department of Chemistry, University of Leicester.

§ Current address: Institute of Biochemistry and Biophysics, University of Tehran, Tehran, Iran.

‖ Department of Biochemistry, University of Leicester.

[1] Abbreviations: APX, ascorbate peroxidase; rpAPX, recombinant wild-type pea cytosolic APX; rsAPX, recombinant soybean cytosolic ascorbate peroxidase; DME-APX, APX reconstituted with iron(III) protoporphyrin IX dimethyl ester; C*c*P, cytochrome *c* peroxidase; MnP, manganese peroxidase.

10.1021/bi0606849 CCC: $33.50
Published on Web 06/01/2006

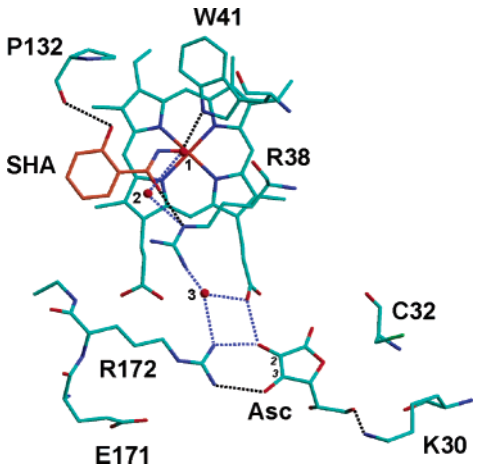

FIGURE 1: Diagram showing the locations of the ascorbate (Asc) and salicylhydroxamic acid (SHA) binding sites in APX (PDB accession codes 1OAF and 1VOH, respectively) (*5*, *6*). Hydrogen bonds are shown as dotted lines. The 2-OH and 3-OH groups of the ascorbate (Scheme 1) are indicated. In addition, a proposed proton transfer pathway from ascorbate to the heme iron is shown (blue dotted lines); the water molecules involved in this proton transfer pathway are indicated as red spheres (labeled 1−3).

with salicylhydroxamic acid (SHA) (Scheme 1), which is an inhibitor for APX but is more soluble than the aromatic substrates; this structure shows SHA binding close to the δ-meso carbon of the heme group (Figure 1). Together, these two structures provided the first information on the possible pathway for proton transfer from the bound ascorbate to the heme, involving discrete water molecules and Arg38 (Figure 1). This was significant because the detailed mechanism of proton transfer is not well established for any heme peroxidase.

With the first ideas beginning to emerge on how substrate binding in APX is controlled, it is timely to begin to dissect the functional role of individual cationic residues either at (Lys30, Arg172) or directly adjacent to (Lys31) the ascorbate binding site. In this paper, we present kinetic and structural data that provide the first comprehensive analysis of the enzyme−substrate interaction in APX, and we use this new information to build a more detailed picture of the proton transfer process. The implications of these data are discussed in terms of our wider understanding of substrate binding and catalysis in other peroxidases.

EXPERIMENTAL PROCEDURES

Materials. Guaiacol, 5,6-*O*-isopropylidene-L-ascorbic acid (Sigma Chemical Co.), L-ascorbic acid, D-ascorbic acid (Aldrich Chemical Co.), 2-phospho-L-ascorbic acid (Fluka), iron(III) protoporphyrin IX dimethyl ester (Porphyrin Products), and all buffers (Fisher) were all of the highest analytical grade (99%+ purity) and were used without further purification. Water was purified by an Elga purelab purification system, and all buffers were filtered (0.2 μm) prior to use. Hydrogen peroxide solutions were freshly prepared by dilution of a 30% (v/v) solution (BDH); exact concentrations were determined using the published absorption coefficient ($\epsilon_{240} = 39.4\ M^{-1}\ cm^{-1}$) (*9*). All molecular biology kits and enzymes were used according to manufacturer's protocols.

Mutagenesis, Protein Expression, and Purification. Recombinant cytosolic pea APX (rpAPX) was expressed as a His-tagged enzyme (*10*) and isolated according to published procedures (*10*, *11*). Site-directed mutagenesis was performed using the Quikchange mutagenesis kit (Stratagene) according to manufacturer's instructions. Mutations were confirmed by DNA sequencing as reported previously (*10*). A number of single, double, and triple variants of rpAPX were prepared at Lys30, Lys31, and Arg172: (i) variants in which the cationic residues are replaced with neutral residues (referred to in this paper as charge neutralization variants, i.e., K30A, K31A, R172A, K30A/K31A, K30A/R172A, K30A/K31A/R172A); (ii) variants in which the cationic residues are replaced with other cationic residues (referred to as charge conservation variants, i.e., K30R, K31R, R172K, K30R/K31R, K30R/R172K); (iii) variants in which the cationic residues are replaced with anionic residues (referred to as charge reversal variants, i.e., K30D, K31D, R172D). All variants were expressed and purified as for wild-type rpAPX (*10*). The wild-type and variant proteins were initially purified as a mixture of apo- and holoproteins and, therefore, required reconstitution with heme according to published procedures (*10*). All variants purified in this way had a Reinheitzahl (R_Z) value of ≥ 2 after purification, as for the wild-type protein. Absorption coefficients for all variants were determined using the pyridine−hemochromogen method (*12*) and are given in Table 1; the absorption coefficient of rpAPX has been reported previously (*13*) (Table 1). In separate experiments, it was found that the K30R/K31R/R172K, K30D/K31D, K30D/R172D, and K30D/K31D/R172D variants could not be reconstituted with excess hemin, as for the wild-type protein and the other variants mentioned above. Attempts to incorporate hemin during expression of the variants in *Escherichia coli* were also unsuccessful, and these variants were not pursued further.

Reconstitution with Iron(III) Protoporphyrin IX Dimethyl Ester rpAPX. Apoenzyme was initially prepared by the method of Teale (*14*). Specifically, the enzyme eluting from the Ni-affinity column (pH 4.2, 100 mM potassium phosphate, 0.3 M potassium chloride) was dialyzed into potassium phosphate (10 mM), pH 7.0, overnight at 4 °C and concentrated to ≈13−20 mg/mL, and the pH was lowered to 1.5 through addition of 1 M HCl with stirring on ice. The heme was extracted through addition of an equal volume of ice-cold butan-2-one (Aldrich) and the organic layer removed; this process was repeated until a straw-colored aqueous apoenzyme-containing layer was observed. The aqueous layer was dialyzed sequentially against 5 L of 1 mM $NaHCO_3$, 5 L of 1 mM EDTA, and finally 5 L of 1 mM $NaHCO_3$ at 4 °C. The apoenzyme was then further dialyzed against 10 mM potassium phosphate (pH 8.5) at 4 °C and concentrated as above.

Iron(III) protoporphyrin IX dimethyl ester (>97%; Porphyrin Products, Frontier Scientific Inc.) was dissolved in dry DMSO (≥99.8%, 1 mg/mL, 1.1 equiv) which was added dropwise to the enzyme solution (90% DMSO, 200 mL), with stirring on ice, and incubated for 20 min. An additional amount of the ester (0.1 equiv) was added and the solution incubated for a further 10 min. This solution was dialyzed against potassium phosphate (20 mM, pH 7.0) overnight at 4 °C. The precipitated protein was collected by centrifugation (3000*g*, 20 min), dissolved (100 mM potassium phosphate, pH 8.0, 10% glycerol), and purified by FPLC (Superdex HR75 column, isocratic gradient 150 mM potassium phosphate buffer, pH 8.0) to remove a small amount of excess

Scheme 1: Structures of Various Substrates Referred to in This Work[a]

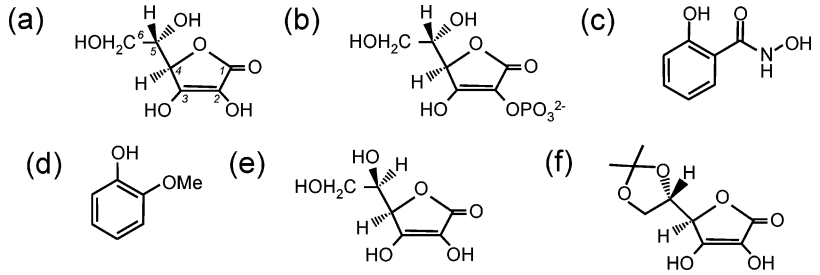

[a] Substrates: (a) L-ascorbic acid, (b) 2-phospho-L-ascorbic acid, (c) salicylhydroxamic acid, (d) guaiacol, (e) D-ascorbic acid, and (f) 5,6-*O*-isopropylidene-L-ascorbic acid.

Table 1: Wavelength Maxima (nm) for the Ferric, Compound I, and Compound II Derivatives of the Variants Examined in This Work[a]

derivative	λ_{max} (nm)		
	ferric	Compound I	Compound II
wild type	408 (88)	411	416
charge neutralization			
K30A	405 (99)	413	419
K31A	406 (103)	410	417
R172A	408 (102)	412	417
K30A/K31A	407 (86)	412	417
K30A/R172A	408 (110)	412	417
K30A/K31A/R172A	408 (119)	412	417
charge conservation			
K30R	406 (82)	410	413
K31R	408 (105)	411	415
R172K	408 (92)	412	417
K30R/K31R	408 (92)	412	416
K30R/R172K	409 (85)	412	416
charge reversal			
K30D	404 (75)	408	411
K31D	407 (75)	411	415
R172D	407 (105)	411	417

[a] Absorption coeffficients for the ferric derivatives (mM^{-1} cm^{-1}) are shown in parentheses.

heme and any other impurities. The purified enzyme, referred to as DME-APX, had a R_Z value of >2.

Steady-State Kinetics. Steady-state measurements (50 mM sodium phosphate, pH 7.0, 25 °C) for ascorbic acid, guaiacol, and cytochrome *c* were carried out according to published protocols (*7*, *15*). For L-ascorbic acid, D-ascorbic acid, and 5,6-*O*-isopropylidene-L-ascorbic acid, initial rates were calculated from time-dependent absorbance changes and multiplied by a factor of 2 to allow for disproportionation of the monodehyroascorbate radical (*7*). Substrate concentrations were calculated using the following absorption coefficients: L-ascorbic acid, ϵ_{290} = 2.8 mM^{-1} cm^{-1} (*16*); guaiacol, ϵ_{470} = 22.6 mM^{-1} cm^{-1} (*17*); D-ascorbic acid, ϵ_{290} = 3.3 mM^{-1} cm^{-1}; 5,6-*O*-isopropylidene-L-ascorbic acid, ϵ_{290} = 4.2 mM^{-1} cm^{-1}; cytochrome *c*, ϵ_{550} = 27.7 mM^{-1} cm^{-1}. Data were fitted to either the Michaelis−Menten or Hill equation, as previously (*7*).

Transient-State Kinetics. Transient-state kinetics (50 mM sodium phosphate, pH 7.0, 10 °C) were performed using a SX.18 MV microvolume stopped-flow spectrophotometer (Applied Photophysics) fitted with a Neslab RTE200 circulating water bath (±0.1 °C). Reported values of k_{obs} are an average of at least three independent measurements. All curve fitting was performed using Kaleidagraph (KaleidaGraph, version 3.09, Synergy Software), and data were analyzed using nonlinear least-squares regression analysis on an Archimedes 410-1 microcomputer using the Spectrakinetics software (Applied Photophysics Ltd.). Time-dependent spectra of the various reactions were obtained by single and sequential mixing, multiple wavelength stopped-flow spectroscopy using a photodiode array detector, and X-scan software (Applied Photophysics Ltd.). Spectral intermediates were isolated using the singular value decomposition by global analysis and numerical integration methods (PROKIN software, Applied Photophysics Ltd.). Pseudo-first-order rate constants for Compound I formation ($k_{1,obs}$), Compound I reduction ($k_{2,obs}$), and Compound II reduction ($k_{3,obs}$) were determined at the ferric Soret maxima, the ferric and Compound II isosbestic, and the ferric and compound I isosbestic, respectively. In all cases, observed changes in absorbance were 96−99% of the calculated values. Second-order rate constants were obtained from a linear plot of k_{obs} against $[H_2O_2]$ or [substrate], respectively. For some variants, observed rate constants for Compound II reduction ($k_{3,obs}$) showed saturation kinetics (*7*), consistent with a mechanism involving preassociation of the substrate (HS) with Compound II (eqs 4 and 5). In this case, values for $k_{3,obs}$ were

$$\text{Compound II} + \text{HS} \overset{K_a}{\rightleftharpoons} [\text{Compound II}-\text{HS}] \quad (4)$$

$$[\text{Compound II}-\text{HS}] \xrightarrow{k_3} \text{ferric} + \text{S}^{\bullet} + \text{H}_2\text{O} \quad (5)$$

fitted to eq 6 to extract the limiting rate constant, k_3, and the equilibrium dissociation constant for the substrate-bound complex, K_d ($K_d = 1/K_a$):

$$k_{3,obs} = k_3/(1 + K_d/[\text{HS}]) \quad (6)$$

where [HS] is the concentration of ascorbate and K_d is the equilibrium dissociation constant for the substrate-bound complex ($K_d = 1/K_a$). In some cases, kinetic data for reduction of Compound II gave monophasic absorbance−time traces at low substrate concentrations but biphasic traces at high substrate concentrations (above ≈600−800 mM), as observed previously for the wild-type protein (*7*). In these cases, data for the first phase of the biphasic traces were used together with the data at low substrate concentrations to compute values for k_3 and K_d.

Protein Crystallography. The R172A variant of recombinant soybean APX was also prepared. Crystals of this R172A mutant were prepared as described previously (*6*). Diffraction data were collected in beamline ID14-EH3 at ESRF (Grenoble) using an ADSC Quantum-4 detector. Data to 1.8 Å was collected over 90° rotation in 1.0° images. All data were collected at 100 K. Data collection statistics are

Table 2: Data Collection and Refinement Statistics for R172A (PDB Accession Code 2CL4)[a]

data collection	
resolution (Å)	28.87−1.80 (1.90−1.80)
total observations	167549
unique reflections	23768
$I/\sigma I$	18.26 (5.34)
R_{merge} (%)	0.071 (0.365)
completeness (%)	98.9
refinement	
R_{work}	0.162
R_{free}	0.199
rmsd from ideal	
bonds (Å)	0.009
angles (deg)	1.145

[a] Values in parentheses refer to the outer bin.

shown in Table 2; 5% of the data were flagged for the calculation of R_{free} and excluded from subsequent refinement. The structure was refined from a model derived from the 1.45 Å rsAPX−ascorbate complex (*6*) (Protein Data Bank accession code 1OAF) by the removal of bound ascorbate, water molecules, and the side chain atoms beyond C^{β} in Arg172. Several cycles of refinement using REFMAC5 (*18*) from the CCP4 suite (*19*) and incorporation of solvent molecules gave a model with a crystallographic *R*-factor for all data of 16.2% and an R_{free} of 19.9%. The electron density for the water molecules that replace the guanidinium group was clear and unambiguous. XtalView (*20*) was used throughout for manual adjustment, ligand fitting, and interpretation of water structure. Final refinement statistics are presented in Table 2.

RESULTS

Electronic Spectra. Wavelength maxima for the ferric derivatives of all variants are indicated in Table 1. In all cases, spectra are similar to those for the wild-type enzyme (*7*), with only small (1−3 nm) shifts in maxima for the Soret band observed. This is consistent with the fact that the amino acid substitutions are on the surface of the protein and not at the heme active site.

Steady-State Oxidation of Aromatic Substrates. Steady-state data for oxidation of guaiacol and L-ascorbic acid by wild-type and site-directed variants are shown in Table 3. The oxidation of guaiacol by all variants obeyed Michaelis−Menten kinetics, and values for both k_{cat} (k_{cat} = 38−140 s^{-1}, compared to k_{cat} = 63 s^{-1} for wild type) and K_M (K_M = 2.2−13 mM, compared to K_M = 14 mM for wild type) were in a similar range to those for the wild-type protein (*7*), indicating that the Arg172, Lys30, and Lys31 mutations have little effect on the ability of the enzyme to oxidize this aromatic substrate.

Steady-State Oxidation of L*-Ascorbate.* Oxidation of L-ascorbic acid does not obey Michaelis−Menten kinetics for any of the enzymes examined in this study, and data were fitted to the Hill equation as previously for the wild-type protein (*7*). Charge neutralization at Lys30 and/or Lys31 (K30A, K31A, K30A/K31A) yielded k_{cat} (k_{cat} = 72−190 s^{-1}) and K_M (K_M = 300−370 mM) values that were of a similar magnitude to that of the wild-type protein (k_{cat} = 80 s^{-1}; K_M = 300 mM). A representative set of data is shown in Figure 2 for the K30A variant. Introduction of an alternative cationic residue (K30R, K31R, K30R/K31R) or charge reversal at the 30 and 31 positions (K30D, K31D) does not have a major impact on the binding (K_M = 220−400 mM) or oxidative turnover (k_{cat} = 82−300 s^{-1}) of ascorbate.

In marked contrast, substantial effects were observed for all variants incorporating mutations at Arg172 (R172A, K30A/R172A, K30A/K31A/R172A; R172K, K30R/R172K; R172D). A representative data set is shown in Figure 2 for the K30A/K31A/R172A variant. For these R172 variants, small but measurable activity was observed, but binding of ascorbate is weak: plots of rate versus substrate concentration were linear because the concentrations of ascorbate needed to reach rate saturation were too high to be experimentally accessible (Figure 2). Values for k_{cat} and K_M could not be obtained for these variants, therefore. Instead, a comparative measure of enzyme activity for these variants can be obtained from the linear slope of the v/[E] versus [substrate] plot: in this case, average values of ≈3−4 mM^{-1} s^{-1} are obtained for all variants containing an R172 mutation, which are ≈100-fold lower than comparable values for the wild-type protein and the various K30/K31 variants (values averaging ≈200 mM^{-1} s^{-1}).

Steady-State Oxidation of Substrate Analogues: D*-Ascorbic Acid and 5,6-O-Isopropylidene-*L*-ascorbic Acid.* With these substrates (Scheme 1), the hydrogen-bonding interaction with Lys30 is disrupted, providing an additional means of assessing the role of this electrostatic interaction. The wild-type enzyme was shown to be competent for oxidation of both substrates, and steady-state parameters were extracted by fitting of the data to the Hill equation (D-ascorbic acid, k_{cat} = 50 ± 5.0 s^{-1}, K_M = 430 ± 60 mM; 5,6-*O*-isopropylidene-L-ascorbic acid, k_{cat} = 51 ± 7.1 s^{-1}, K_M = 1300 ± 270 mM). Oxidation of these two substrates by the R172 variants showed values for k_{cat} averaging ≈5% of the value for the wild-type enzyme, which is as expected since the (major) interaction with R172 is missing. For the K30/K31 variants, values for k_{cat} were similar to those for the wild-type enzyme (k_{cat} ≈ 50−150% of wild type); this is also as expected since the (minor) hydrogen bond interaction with Lys is the only one disrupted in both cases.

Removal of the Heme Propionate Interaction. The above observations indicate that the hydrogen bond to Lys30 is far less influential for stabilization of the APX−ascorbate complex than that to Arg172 but that the enzyme is still capable of ascorbate activity even in the absence of both hydrogen bonds (albeit at a much reduced level). To assess the role of the one remaining hydrogen bond interaction, that between the substrate and the heme propionate (Figure 1), the enzyme was reconstituted with iron(III) protoporphyrin IX dimethyl ester in which both propionates of the heme group are replaced with ester groups (DME-APX). Wavelength maxima for ferric DME-APX (λ_{max} = 409, 522, 562, 602 nm) were similar to those for the wild-type enzyme and are consistent with a predominantly five-coordinate high-spin iron. Under the same conditions as used for the wild-type protein, DME-APX was found to oxidize guaiacol (k_{cat} = 0.7 ± 0.004 s^{-1}, K_M = 13 ± 1.6 mM). In control experiments under the same conditions, oxidation of guaiacol by iron(III) protoporphyrin IX dimethyl ester alone was not observed. In contrast, no measurable activity toward L-ascorbate could be detected for DME-APX under any conditions. In further experiments, ascorbate assays were also carried out at elevated concentrations of DME-APX (up to

Table 3: Steady-State Kinetic Parameters for Oxidation of L-Ascorbic Acid and Guaiacol

	L-ascorbic acid[a]		guaiacol[b]	
enzyme	k_{cat} (s^{-1})	K_M (μM)	k_{cat} (s^{-1})	K_M (mM)
wild type	80 ± 6.0	300 ± 29	63 ± 1.6	14 ± 0.7
charge neutralization				
K30A	190 ± 11	320 ± 30	95 ± 4.0	11 ± 1.0
K31A	140 ± 10	370 ± 38	110 ± 5.0	13 ± 1.0
R172A	–	–	38 ± 8.0	6.0 ± 0.7
K30A/K31A	72 ± 3.5	300 ± 21	88 ± 3.0	11 ± 1.0
K30A/R172A	–	–	77 ± 3.0	4.0 ± 0.4
K30A/K31A/R172A	–	–	120 ± 4.0	6.0 ± 0.6
charge conservation				
K30R	300 ± 28	400 ± 50	140 ± 11	12 ± 1.8
K31R	200 ± 14	430 ± 37	54 ± 3.0	9.7 ± 1.2
R172K	–	–	82 ± 6.0	3.9 ± 0.8
K30R/K31R	120 ± 11	220 ± 31	57 ± 4.0	12 ± 1.7
K30R/R172K			76 ± 5.0	5.0 ± 0.8
charge reversal				
K30D	110 ± 9.0	400 ± 80	110 ± 10	12 ± 1.9
K31D	82 ± 4.0	290 ± 15	83 ± 5.0	12 ± 1.5
R172D	–	–	75 ± 4.0	2.2 ± 0.3

[a] Data fitted using the Hill equation. [b] Data fitted using the Michaelis–Menten equation (*7*).

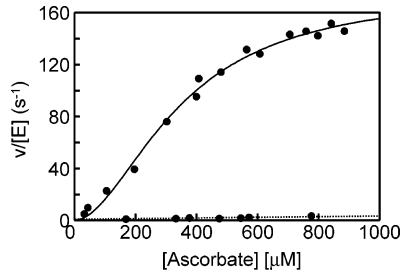

FIGURE 2: Steady-state oxidation of L-ascorbate by K30A (solid line) and K30A/K31A/R172A (dotted line). Data for K30A were fitted to the Hill equation, as previously for the wild-type protein (*7*); data for K30A/K31A/R172A were fitted to $y = mx + c$.

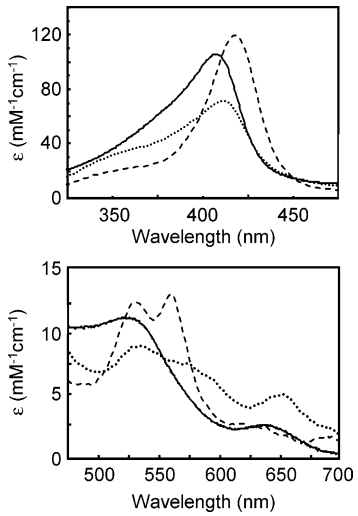

FIGURE 3: Top: UV–visible spectra in the Soret region of ferric R172D (solid line) and its oxidized Compound I (dotted line) and Compound II (dashed line) intermediates. Bottom: The corresponding spectra in the visible region.

1.5 μM, which is 1000-fold higher than the concentration used for all other assays): even under these conditions, no ascorbate activity was detected.

Pre-Steady-State Kinetics. Wavelength maxima for the Compound I and II intermediates of all variants were obtained using photodiode array experiments; wavelength maxima are given in Table 1, and representative spectra for the R172D variant are presented in Figure 3. All variants are competent for formation of the key catalytic intermediates, Compounds I and II, as evidenced by the similarity of intermediate spectra to those for the wild-type protein.

Observed pseudo-first-order rate constants ($k_{1,obs}$) for Compound I formation (eq 1) showed a linear dependence on H_2O_2 concentration for all variants. Second-order rate constants, k_1, obtained from the slope of a plot of $k_{1,obs}$ against [H_2O_2] concentration, are given in Table 4. All rate constants are similar to those observed for the wild-type enzyme, indicating that these (surface) mutations do not affect the mechanism of Compound I formation.

Second-order rate constants for Compound I reduction, k_2 (eq 2), are shown in Table 4 and mirror the observations found in steady-state experiments. In all cases, a linear dependence of $k_{2,obs}$ on [ascorbate] is observed. Charge neutralization (K30A, K31A, K30A/K31A), charge conservation (K30R, K31R, K30R/K31R), or charge reversal (K30D, K31D) at Lys30 and/or Lys31 has little influence on k_2, whereas all mutations involving Arg172 have a more substantial effect ($k_2 \approx 5-10$-fold lower than wild type).

For the wild-type enzyme, reduction of Compound II is rate-limiting in the overall mechanism, and a nonlinear dependence on [substrate] is observed that is consistent with preassociation of the substrate with Compound II (K_d) prior to electron transfer, k_3 (eqs 4 and 5). All of the variants examined in this work are competent for reduction of Compound II. For the K30/K31 charge neutralization, charge conservation, and charge reversal variants, nonlinear kinetics are also observed, as for the wild-type protein, and first-order limiting rate constants, k_3, and binding constants, K_d, were derived (eq 6 and Table 4). Representative data sets are shown in Figure 4. For these variants, values of k_3 and K_d are similar to those obtained for the wild-type enzyme, in agreement with the steady-state data above. In contrast, variants incorporating a R172 mutation display a linear dependence on ascorbate concentration over a comparable concentration range, and rate saturation is not observed

Table 4: Rate Constants for Formation (k_1) and Reduction (k_2) of Compound I and for Reduction of Compound II (k_3)[a]

enzyme	formation of Compound I, k_1 ($\times 10^7$ M^{-1} s^{-1})	reduction of Compound I, k_2 ($\times 10^6$ M^{-1} s^{-1})	reduction of Compound II[b]		
			k_3 (s^{-1})	K_d (μM)	k_3' (mM^{-1} s^{-1})
wild type	6.8 ± 0.11	36 ± 0.30	30 ± 3	75 ± 20	−
charge neutralization					−
K30A	5.0 ± 0.12	28 ± 0.22	18 ± 1.4	72 ± 7.1	−
K31A	6.9 ± 0.07	30 ± 0.06	34 ± 3.0	200 ± 33	
R172A	6.3 ± 0.08	4.3 ± 0.07	−	−	4.1 ± 0.036
K30A/K31A	3.6 ± 0.02	20 ± 0.42	30 ± 3.2	320 ± 73	−
K30A/R172A	6.7 ± 0.08	4.4 ± 0.03	−	−	2.7 ± 0.010
K30A/K31A/R172A	3.8 ± 0.03	3.6 ± 0.01	−	−	3.2 ± 0.30
charge conservation					
K30R	6.4 ± 0.05	37 ± 3.6	47 ± 6.5	380 ± 85	−
K31R	3.0 ± 0.06	61 ± 1.2	10 ± 0.31	14 ± 2.0	−
R172K	5.9 ± 0.02	7.2 ± 0.28	−	−	6.8 ± 0.14
K30R/K31R	3.3 ± 0.07	60 ± 0.60	14 ± 0.86	160 ± 23	−
K30R/R172K	4.3 ± 0.08	8.5 ± 0.23	−	−	3.7 ± 0.034
charge reversal					
K30D	6.3 ± 0.05	11 ± 0.11	26 ± 2.4	100 ± 20	−
K31D	6.6 ± 0.11	27 ± 0.37	14 ± 0.80	48 ± 8.4	−
R172D	7.0 ± 0.11	4.2 ± 0.07	−	−	11.8 ± 0.56

[a] Values for k_1, k_2, and k_3 were determined at the ferric Soret maximum, the ferric/Compound II isosbestic, and the ferric/Compound I isosbestic, respectively (*7*). These maxima were at the following wavelengths (nm): wild type, 408, 411, 422; K30A, 405, 409, 419; K31A, 406, 410, 421; R172A, 408, 412, 421; K30A/K31A, 407, 410, 421; K30A/R172A, 408, 409, 420; K30A/K31A/R172A, 408, 411, 421; K30R, 406, 411, 421; K31R, 408, 413, 418; R172K, 408, 411, 424; K30R/K31R, 408, 411, 421; K30R/R172K, 409, 413, 421; K30D, 404, 409, 421; K31D, 407, 411, 421; R172D, 407, 411, 421. [b] Data either showed saturation kinetics (wild type and K30/K31 variants) and were fitted to eq 6 to yield values for k_3 and K_d (*7*) or showed linear kinetics (R172 variants) and were fitted to $y = mx + c$ to yield the second-order rate constant k_3' (for comparison, the value for k_3' extracted from the linear part of the nonlinear dependence for the wild-type protein is 364 mM^{-1} s^{-1}).

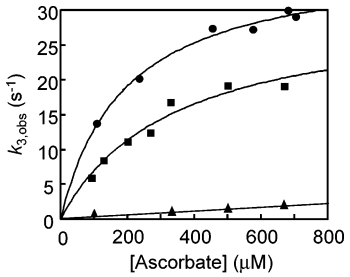

FIGURE 4: Plot of the pseudo-first-order rate constant, $k_{3,obs}$, versus [L-ascorbic acid] for the reduction of Compound II by wild type (●), K30A/K31A (■), and K30A/R172A (▲). The data for wild type and K30A/K31A are fitted to eq 6; the data for K30A/R172A are fitted to $y = mx + c$.

(Figure 4). Binding of ascorbate must therefore be much weaker in these variants (estimated $K_d \gg 2$ mM), which confirms the observations in the steady state. For these variants, second-order rate constants (k_3') are extracted instead from the linear dependence of $k_{3,obs}$ versus [substrate] and are in the range ≈2−12 mM^{-1} s^{-1} (Table 4); for comparison, the value for k_3' extracted from the linear part of the nonlinear dependence for the wild-type protein is ≈100-fold higher (364 mM^{-1} s^{-1}).

X-ray Crystallography. Crystals of the R172A variant of recombinant soybean APX (rsAPX)[2] were obtained under the same conditions as the wild-type protein (*14*). The structure was refined using data to 1.8 Å; the final *R*-factor (all data) is 0.162 (data collection and refinement statistics are shown in Table 2). Figure 5 shows the electron density of the R172A variant in the region of the mutation. The overall structure of the enzyme is unaffected by the mutation. The electron density for the side chain of Lys30 is poor beyond C^β in R172A, and this residue is presumed to be disordered in the crystal structure. This residue is not oriented toward the substrate binding site, confirming the observation (*6*) made in the structure of the wild-type protein in the absence of substrate. Comparison of the R172A crystallographic data (Figure 6a) with the structure of the wild-type enzyme (Figure 6b) indicates that solvent molecules (labeled 4 and 5 in Figure 6a) occupy the same site as the original guanidinium group of the Arg172 side chain. There are four solvent water molecules observed in the wild-type structure (labeled 6−9 in Figure 6b) that are displaced on binding of substrate (Figure 6c); these four solvent molecules are also present in the same position in the R172A structure, although one of them (labeled 7) is displaced slightly.

The kinetic data above indicate that the interaction of the substrate with Arg172 is more influential than that with Lys30 but that variants in which Arg172 is missing still retain measurable activity toward ascorbate. These data, together with the kinetic data for DME-APX, suggest that the hydrogen-bonding interaction to the heme propionate is a key determinant and that if this interaction exists, then some catalytic activity remains. Catalytic turnover also requires the existence of a competent proton transfer pathway, however, because reduction of Compound II (eq 3) requires release of the ferryl oxygen as H_2O. For the wild-type protein, a possible proton transfer pathway from C^2 of the substrate (Scheme 1, Figure 1) to the heme iron has been identified (*19*) that involves Arg38 and three discrete water molecules (labeled 1−3 in Figures 1 and 6). The crystallographic data

[2] The rsAPX enzyme has >90% sequence identity to the rpAPX enzyme; rsAPX contains the conservative K30R substitution; the crystal structure of rsAPX shows that R30 overlays closely with K30 in rpAPX (*21*). We have not been able to crystallize rpAPX or any variants of rpAPX isolated using the His-tag expression vector (*10*). In control experiments, the R172A variant of rsAPX was shown to duplicate the properties of the equivalent R172A variant in rpAPX [λ_{max}(ferric) = 408 nm (Table 1); $k_{cat} = 0.98 \pm 0.10$ s^{-1}, $K_M = 310 \pm 55$ μM (Table 3)]. We have been unable to obtain crystals of R172A with ascorbate bound.

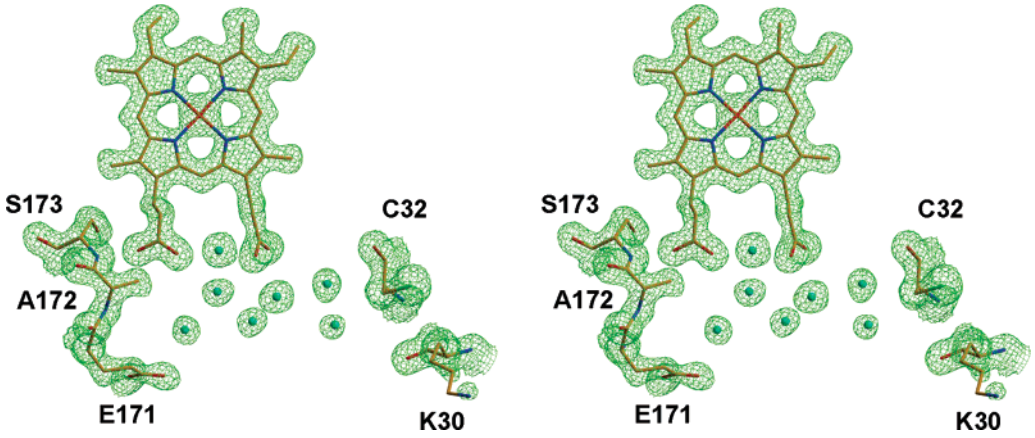

FIGURE 5: Stereoview of the R172A variant of rsAPX (PDB accession code 2CL4) in the region of the heme and ascorbate binding site, showing refined electron density (green). The figure was prepared with XtalView (*20*) and Raster3D (*27*).

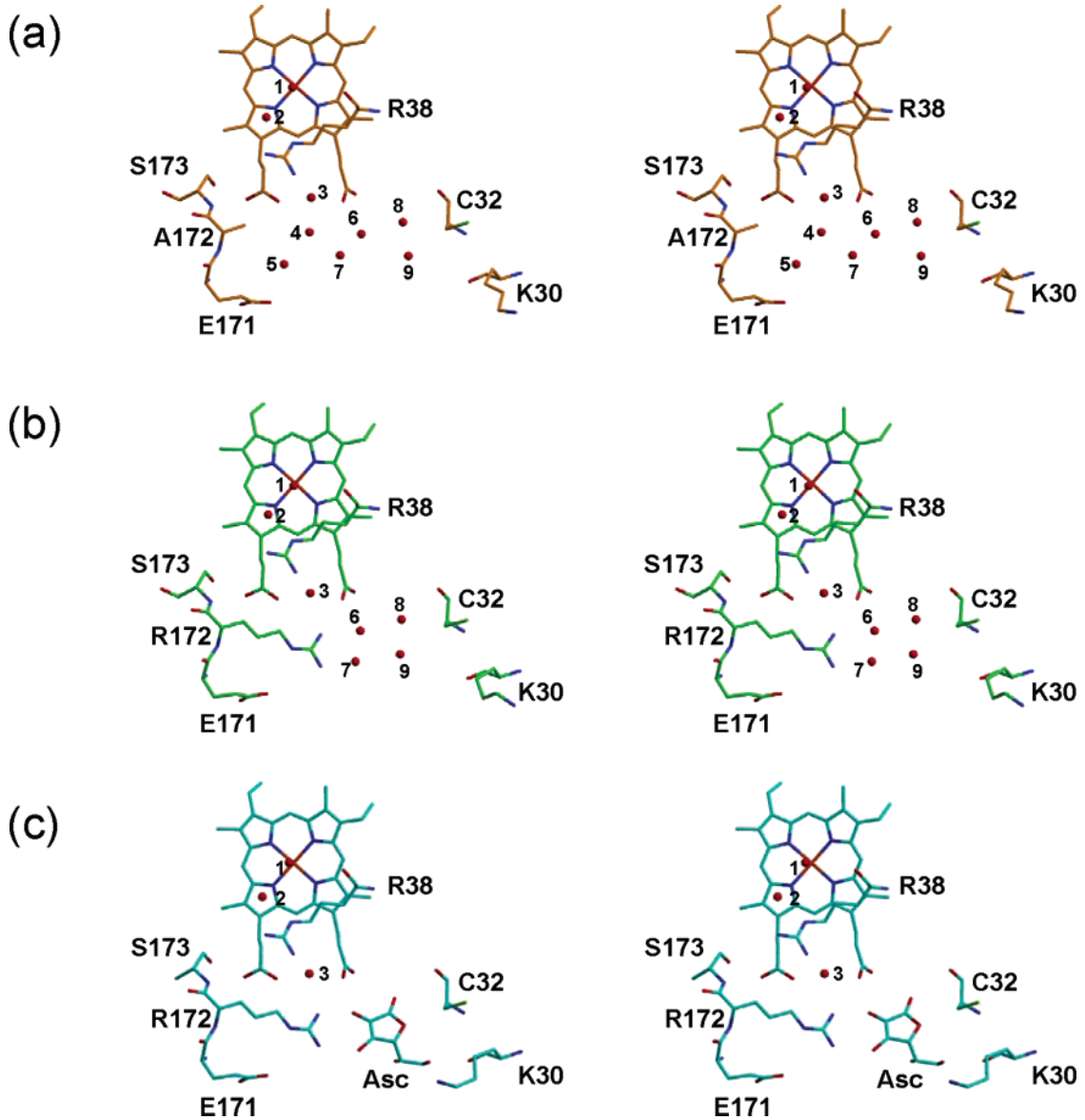

FIGURE 6: Structures of (a) the R172A variant of rsAPX (PDB accession code 2CL4), (b) wild-type APX rsAPX (PDB accession code 1OAG), and (c) the APX−ascorbate complex (PDB accession code 1OAF) in the region of the ascorbate binding site. Water molecules are shown as red spheres and are labeled 1−9. The figure was prepared with XtalView (*20*) and Raster3D (*27*).

for R172A indicate that the essential components of this proton transfer pathway are intact in this variant because water molecules 1−3 are preserved and because Arg38 overlays directly with Arg38 in the wild-type protein. These data indicate that proton transfer to the heme of Compound II is still possible in R172A, in agreement with the pre-

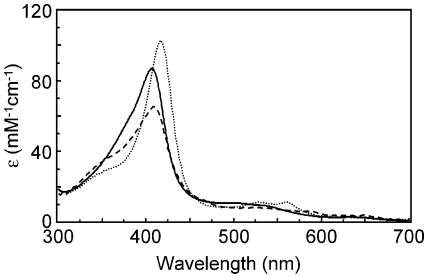

FIGURE 7: Spectra of the intermediates formed on reaction of wild-type APX with 2-phospho-L-ascorbic acid: solid line, the ferric enzyme at $t = 0$; dashed line, the Compound I intermediate formed by reaction of the ferric enzyme with 1.1 equiv of H_2O_2; dotted line, the Compound II intermediate formed from the reaction of Compound I with 1.1 equiv of 2-phospho-L-ascorbic acid. On addition of further (up to 10) equivalents of 2-phospho-L-ascorbic acid, no further changes in the spectrum of Compound II were observed.

steady-state kinetic data for this variant, and are consistent with the steady-state data in which catalytic turnover of ascorbate is clearly observed.

Turnover of Substrate Analogues: 2-Phospho-L-ascorbic Acid. The above kinetic and structural data indicated that substrate binding, albeit weak, occurs in the absence of Lys30 and Arg172 and that proton transfer from ascorbate to the heme iron was still possible in these variants. To probe the molecular details of the proton transfer process in further detail, oxidation of 2-phospho-L-ascorbate (Scheme 1) was investigated. For this compound, electron transfer is possible but proton transfer from the substrate to the heme iron is not because the proton donor (the C^2 group of L-ascorbate, Scheme 1) is missing. Compound I of the wild-type enzyme was quantitatively converted to Compound II ($\lambda_{max} = 417$, 528, 560 nm), which is in agreement with literature values [$\lambda_{max} = 417$, 529, 560 nm (*7*)] by addition of 1 equiv of 2-phospho-L-ascorbate (Figure 7), indicating that binding of 2-phospho-L-ascorbate to the enzyme is possible and that electron transfer to the heme can occur. However, further reaction of the Compound II product with additional equivalents (up to 10 equiv) of 2-phospho-L-ascorbate did not reduce Compound II back to the native ferric state (in control experiments, under the same conditions, Compounds I and II of the wild-type enzyme are quantitatively reduced by 1 equiv of ascorbate). In separate steady-state experiments (data not shown), no change in absorbance (in the range 200−300 nm) corresponding to oxidation of this substrate was observed, even though formation of Compound II could be detected (200−700 nm), indicating that steady-state turnover of this substrate does not occur.

DISCUSSION

The working model that has emerged (*5*, *6*, *22*, *23*) for oxidation of different types of substrate by ascorbate peroxidase is as follows. There are two, separate binding locations. The first, used by ascorbate, is close to the heme 6-propionate group (Figure 1). The second is used by aromatic substrates (e.g., guaiacol, *p*-cresol); its location has not been unambiguously confirmed but is likely to be close to the δ-heme edge (Figure 1). The variants examined in this work have little influence on oxidation of aromatic substrates, as evidenced by steady-state data for guaiacol oxidation. This confirms the working model of two substrate binding sites, with the two sites functioning independently of one another.

The kinetic data for oxidation of ascorbate are more intriguing. Both steady-state and pre-steady-state data (Tables 3 and 4) show that mutations at Lys30 are much less disruptive than those at Arg172. Hence, charge neutralization, charge reversal, or charge conservation at Lys30 has little effect on the ability of the enzyme to bind (as evidenced by K_M) or turnover (as evidenced by k_{cat}) ascorbate; pre-steady-state data (Table 4) confirm these observations and show that reduction of Compounds I and II is largely unaffected by these mutations. Several key points emerge. First, ascorbate binding is not dramatically affected by removal of the hydrogen bond to Lys30. We conclude that the hydrogen bond interaction between ascorbate and Lys30 has a relatively minor role and provides no substantial energetic advantage on substrate binding [we note that in the substrate-free form Lys30 is also within hydrogen-bonding distance (3.5 Å) of Asp29, which presumably provides some energetic stabilization in the absence of substrate]. Second, the substrate binding site is not markedly sensitive to changes in electrostatics because charge substitutions, including charge reversal, at (Lys30) or adjacent to (Lys31) the binding site do not substantially disrupt ascorbate binding.

Of the three hydrogen bonds between the bound ascorbate and the enzyme, the steady-state and pre-steady-state kinetic data show that those to Arg172 are the most influential and have a major role in controlling substrate binding. Replacement of Arg172, to either a neutral residue (R172A), an anionic residue (R172D), or another cationic residue (R172K),[3] leads to a sharp decrease in the ability of the enzyme to bind ascorbate, such that the value for K_M (steady state) or K_d (pre steady state) is now experimentally inaccessible. Additional mutations at Lys30 and/or Lys31 within the existing R172X framework do not lead to further substantial changes, which is consistent with the independent observations for the Lys30/Lys31 variants (vide supra).

The kinetic data for variants in which both Lys30 and Arg172 are removed clearly indicate that substrate binding is still possible when Arg172 and Lys30 are both missing. We conclude, therefore, that the binding site remains competent for ascorbate binding in the absence of *both* Arg172 and Lys30. Our failure to detect any ascorbate activity for DME-APX, in which the hydrogen bond to the heme propionate is missing, while guaiacol activity is clearly observable, supports this conclusion and indicates that this hydrogen bond interaction is a major determinant.

These data are useful in terms of our wider understanding of ascorbate binding across the APX family. Sequence analysis of APX homologues indicates that Lys30 is not conserved across all APXs (*24*). Where Lys30 is not present, it is replaced by a Lys residue at position 31 or 29; in some cases, e.g., the membrane-bound enzyme from spinach, no Lys residue is present at all (but Arg172 is present). Hence, Lys30 (or an equivalent residue at Lys31/Lys29) may not be critical for ascorbate oxidation in all cases, which would be consistent with our observations. Arg172 itself is conserved across all proposed APX homologues, with the exception of the membrane-bound enzyme from *Mesembry-*

[3] The R172K single variant has been isolated previously (*22*).

anthemum crystallinum [Arg172 replaced with an Ile (*24*)] and the enzyme from *Leishmania major* [Arg172 replaced with a Phe (*25*)]. Our data indicate that Arg172 is highly influential and that without it ascorbate binding is dramatically diminished. We note that binding of ascorbate in the *L. major* enzyme is also very weak and that complete steady-state profiles cannot be generated (*25*) (as for our R172X variants), which suggests that the predominant biological role of the *L. major* enzyme may not, in fact, be ascorbate binding.

Catalytic turnover requires more than simply substrate binding at the correct site, however; electron transfer from the substrate to the heme (presumed to occur through the heme 6-propionate) and proton transfer to release the ferryl oxygen as H_2O (eq 3) must also occur. Having dealt with the question of substrate binding (above), we now turn our attention to the question of how efficient oxidation of ascorbate and reduction of Compounds II are achieved for the variants examined in this work. For the K30/K31 variants, which retain normal catalytic activity, we assume that binding of ascorbate and reduction of Compound II occur as in the wild-type protein. Although they bind ascorbate much more weakly, the R172X variants are still competent for reduction of Compound I and Compound II (although the latter at a much reduced level), which allows residual catalytic activity to be maintained. For the wild-type protein, a possible proton transfer pathway has been suggested (*19*) that involves the C^2 group of L-ascorbate and discrete water molecules (Figure 1). That neither reduction of Compound II by 2-phospho-L-ascorbate nor steady-state turnover with this substrate can be observed, while reduction of Compound I by the same compound is still possible, provides further evidence for the involvement of the C^2 group of L-ascorbate in the proton transfer pathway. In addition, the crystallographic data for the R172A (Figures 5 and 6) variant provide further insight: they establish that the essential components of this proton transfer pathway remain intact in R172A because the key solvent water molecules (labeled 1−3 in Figure 6) are preserved and because Arg38 does not change its orientation. Together, these structural data provide sensible rationalization for the low level of activity observed in the R172 variants and the ability of R172A to effect Compound II reduction, by showing that a route for proton transfer from the substrate to the heme is, in principle, still possible in R172A (and by implication in the other Arg172/Lys30 variants).

Finally, we draw attention to the wider issue of how substrate binding specificity is controlled across the family of heme peroxidases. When the structure of the APX−ascorbate complex first appeared, it revealed similarities to the Mn^{2+} site in manganese peroxidase (MnP) and differences with the structural architecture in C*c*P around the substrate binding site. (i) In the case of MnP, the same heme 6-propionate is used for binding of the substrate, along with three anionic residues (Glu35, Glu39, Asp179) and two water molecules (*26*) that are adjacent to the heme 6-propionate. (ii) For C*c*P, the structural differences could be used to rationalize the different substrate specificities (*6*). Attention focused on a cluster of anionic residues (Glu32, Asp33, Asp34, Glu35, Asp37) in C*c*P that are located in or close to a loop region (residues 34−41) and that are used for binding of (cationic) cytochrome *c*. With the exception of Glu32 (which has Glu29 as the equivalent residue in APX), these anionic residues are not present in APX (Scheme 2). [Conversely, the cationic residues (Arg172, Lys30) required for binding of anionic ascorbate in APX are missing in C*c*P (replaced by Asn184 and Asp33).] Since the presence of a cluster of anionic residues appears to be important for binding of both Mn^{2+} in MnP and cytochrome *c* in C*c*P, it is of interest to comment on whether the charge reversal APX variants show increased activity toward either MnP or cytochrome *c*; no such increase could be detected for the K30D, K31D, and K31D/K30D variants examined in this work. Reproduction of the substrate binding properties of other peroxidases will clearly require more subtle modifications.

Scheme 2: Structure-Based Alignment of rpAPX and C*c*P in the Region of the Ascorbate Binding Site

```
          23                                  45
CcP:  YNAIALKLREDDEYDNYIGYGPV

pAPX: KRKLRGFIAEK------K----------CAPL
          20                                  35
```

ACKNOWLEDGMENT

We thank Mr. Kuldip Singh for technical assistance and Dr. David Leys for data collection.

REFERENCES

1. Welinder, K. G. (1992) Superfamily of plant, fungal and bacterial peroxidases, *Curr. Opin. Chem. Biol. 2*, 388−393.
2. Dalton, D. A. (1991) Ascorbate peroxidase, in *Peroxidases in Chemistry and Biology* (Everse, J., Everse, K. E., and Grisham, M. B., Eds.) pp 139−154, CRC Press, Boca Raton, FL.
3. Raven, E. L. (2003) Understanding functional diversity and substrate specificity in haem peroxidases: what can we learn from ascorbate peroxidase?, *Nat. Prod. Rep. 20*, 367−381.
4. Sharp, K. H., Moody, P. C. E., and Raven, E. L. (2003) Defining substrate specificity in haem peroxidases, *Dalton Trans.*, 4208−4215.
5. Sharp, K. H., Moody, P. C. E., Brown, K. A., and Raven, E. L. (2004) Crystal structure of the ascorbate peroxidase-salicylhydroxamic acid complex, *Biochemistry 43*, 8644−8651.
6. Sharp, K. H., Mewies, M., Moody, P. C. E., and Raven, E. L. (2003) The crystal structure of the ascorbate peroxidase/ascorbate complex, *Nat. Struct. Biol. 10*, 303−307.
7. Lad, L., Mewies, M., and Raven, E. L. (2002) Substrate binding and catalytic mechanism in ascorbate peroxidase: evidence for two ascorbate binding sites, *Biochemistry 41*, 13774−13781.
8. Pelletier, H., and Kraut, J. (1992) Crystal structure of a complex between electron transfer partners, cytochrome *c* peroxidase and cytochrome *c*, *Science 258*, 1748−1755.
9. Nelson, D. P., and Kiesow, L. A. (1972) *Anal. Biochem. 49*, 474−478.
10. Metcalfe, C. L., Ott, M., Patel, N., Singh, K., Mistry, S. C., Goff, H. M., and Raven, E. L. (2004) Autocatalytic formation of green heme: evidence for H_2O_2-dependent formation of a covalent methionine-heme linkage in ascorbate peroxidase, *J. Am. Chem. Soc. 126*, 16242−16248.
11. Lad, L., Mewies, M., Basran, J., Scrutton, N. S., and Raven, E. L. (2002) The role of histidine 42 in ascorbate peroxidase: kinetic analysis of the H42A and H42E variants, *Eur. J. Biochem. 369*, 3182−3192.
12. Antonini, M., and Brunori, E. (1971) *Hemoglobin and Myoglobin and their Reactions with Ligands*, North-Holland Publishers, Amsterdam.
13. Hill, A. P., Modi, S., Sutcliffe, M. J., Turner, D. D., Gilfoyle, D. J., Smith, A. T., Tam, B. M., and Lloyd, E. (1997) Chemical, spectroscopic and structural investigation of the substrate-binding site in ascorbate peroxidase, *Eur. J. Biochem. 248*, 347−354.
14. Teale, F. W. J. (1959) Cleavage of the haem-protein link by acid methylethylketone, *Biochim. Biophys. Acta 35*, 543.

15. Kang, D. S., and Erman, J. E. (1982) The cytochrome *c* peroxidase-catalyzed oxidation of ferrocytochrome *c* by hydrogen peroxide. Steady-state kinetic mechanism, *J. Biol. Chem. 257*, 12775−12779.
16. Asada, K. (1984) *Methods Enzymol. 105*, 422−427.
17. Santimone, M. (1975) Titration study of guaiacol oxidation by horseradish peroxidase, *Can. J. Biochem. 53*, 649−657.
18. Murshudov, G. N., Vagin, A. A., and Dodson, E. J. (1997) Refinement of macromolecular structures by the maximum-likelihood method, *Acta Crystallogr. D53*, 240−255.
19. Collaborative Computational Project, Number 4 (1994) The CCP4 suite: programs for protein crystallography, *Acta Crystallogr. D50*, 760−763.
20. McRee, D. (1992) A visual protein crystallographic software system for X11/Xview, *J. Mol. Graphics 10*, 44−47.
21. Patterson, W. R., and Poulos, T. L. (1995) Crystal structure of recombinant pea cytosolic ascorbate peroxidase, *Biochemistry 34*, 4331−4341.
22. Bursey, E. H., and Poulos, T. L. (2000) Two substrate binding sites in ascorbate peroxidase: the role of arginine 172, *Biochemistry 39*, 7374−7379.
23. Mandelman, D., Jamal, J., and Poulos, T. L. (1998) Identification of two-electron transfer sites in ascorbate peroxidase using chemical modification, enzyme kinetics, and crystallography, *Biochemistry 37*, 17610−17617.
24. Jespersen, H. M., Kjaersgard, I. V. H., Ostergaard, L., and Welinder, K. G. (1997) From sequence analysis of three novel ascorbate peroxidases from *Arabidopsis thaliana* to structure, function and evolution of seven types of ascorbate peroxidase, *Eur. J. Biochem. 326*, 305−310.
25. Adak, S., and Datta, A. K. (2005) Leishmania major encodes an unusual peroxidase that is a close homologue of plant ascorbate peroxidase: a novel role of the transmembrane domain, *Biochem. J. 390*, 465−474.
26. Sundaramoorthy, M., Kishi, K., Gold, M. H., and Poulos, T. L. (1994) The crystal structure of manganase peroxidase from *Phanerochaete crysosporium* at 2.06Å resolution, *J. Biol. Chem. 269*, 32759−32767.
27. Merrit, E. A., and Murphy, M. E. P. (1994) Raster3D Version 2.0—A program for photorealistic molecular graphics, *Acta Crystallogr. D50*, 869−873.

BI0606849